Supplementary Information for

Topological insulating states in 2D transition metal dichalcogenides induced by defects and strain

Xiaoyin Li,[a, b, c] Shunhong Zhang,[a] and Qian Wang*[a, b, c]

[a] Center for Applied Physics and Technology, College of Engineering, Peking University; Key Laboratory of High Energy Density Physics Simulation, Ministry of Education, Beijing 100871, China.

[b] Department of Materials Science and Engineering, College of Engineering, Peking University, Beijing 100871, China.

[c] Collaborative Innovation Center of IFSA (CICIFSA), Shanghai Jiao Tong University, Shanghai 200240, China.

Contents

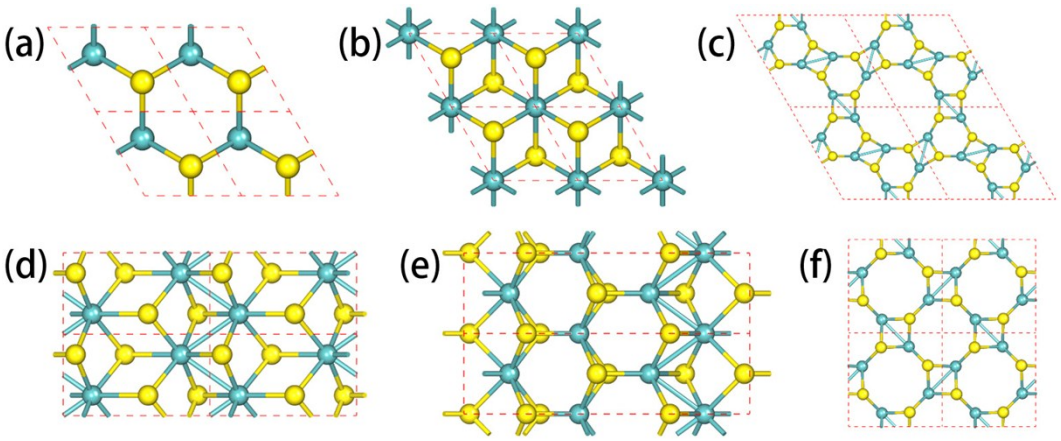

Figure S1. Optimized structures of (a) H-MoS_2, (b) 1T-MoS_2, (c) H′-MoS_2, (d) 1T′-MoS_2, (e) T′′-MoS_2 and (f) so-MoS_2.

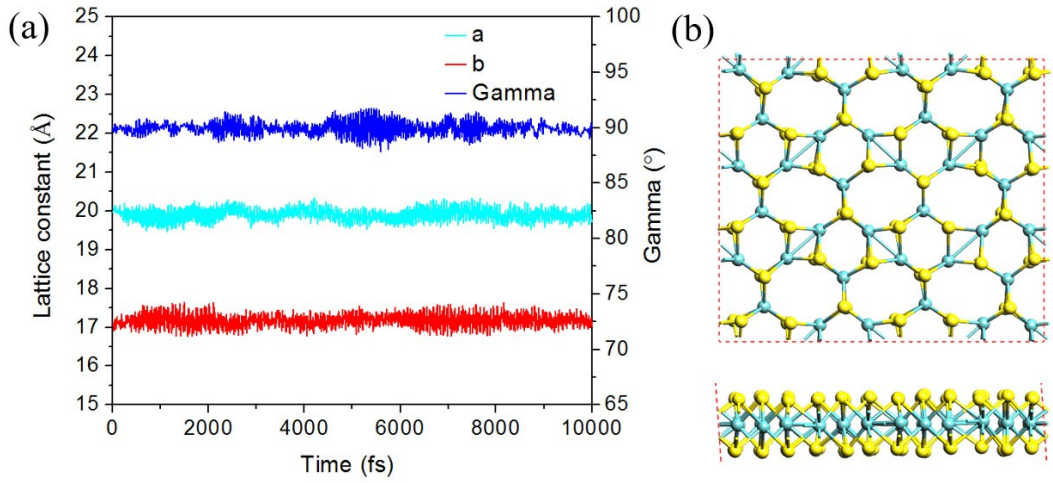

Figure S2. (a) Evolution of lattice parameters a, b, and γ of sho-MoS_2 during the NpT-AIMD simulation at temperature of 300 K. (b) Snapshots of the structure (2×3 supercell) at the end of the simulation.

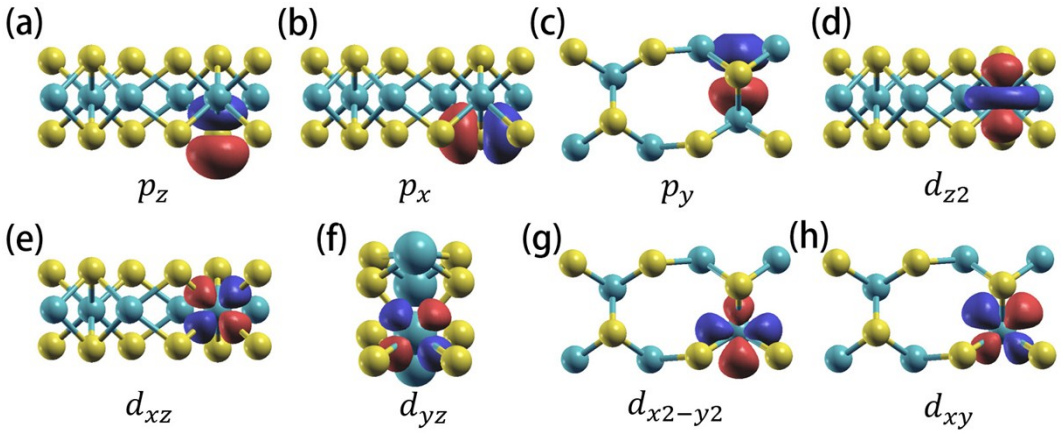

Figure S3. Maximally Localized Wannier functions (MLWFs) of sho-MoS_2, including three S-3p orbitals and five Mo-4d orbitals.

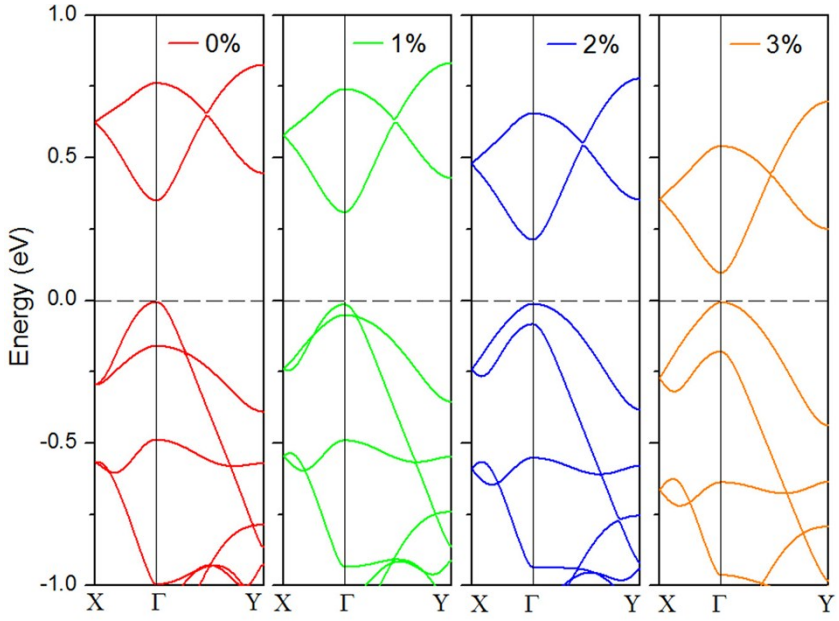

Figure S4. Electronic band structure of sho-MoS_2 under different magnitudes of equi-biaxial tensile strain at the PBE level.

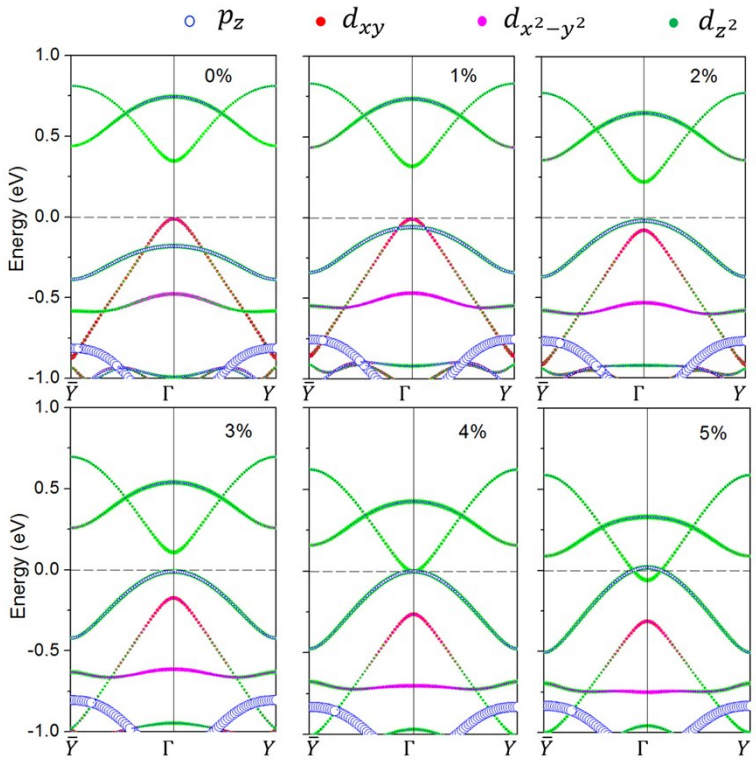

Figure S5. Orbital projected band structure of sho-MoS_2 under different magnitudes of equi-biaxial tensile strains.

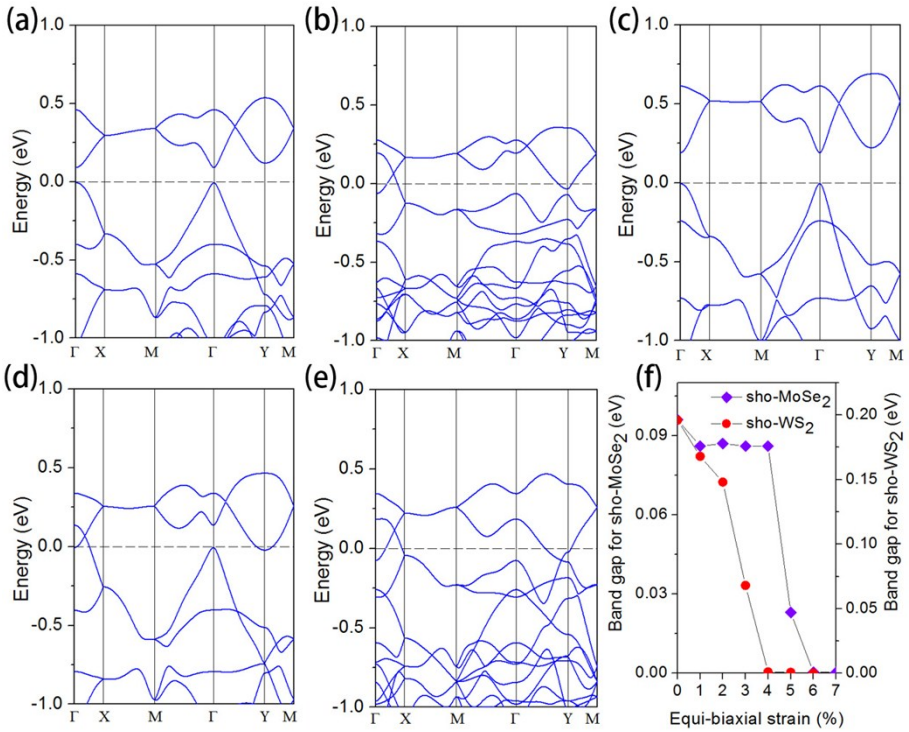

Figure S6. Electronic band structure of (a) sho-$MoSe_2$, (b) sho-$MoTe_2$, (c) sho-WS_2, (d) sho-WSe_2, and (e) sho-WTe_2 calculated using the PBE functional. (f) Energy band

gap as a function of equi-biaxial tensile strain for sho-$MoSe_2$ and sho-WS_2, respectively.

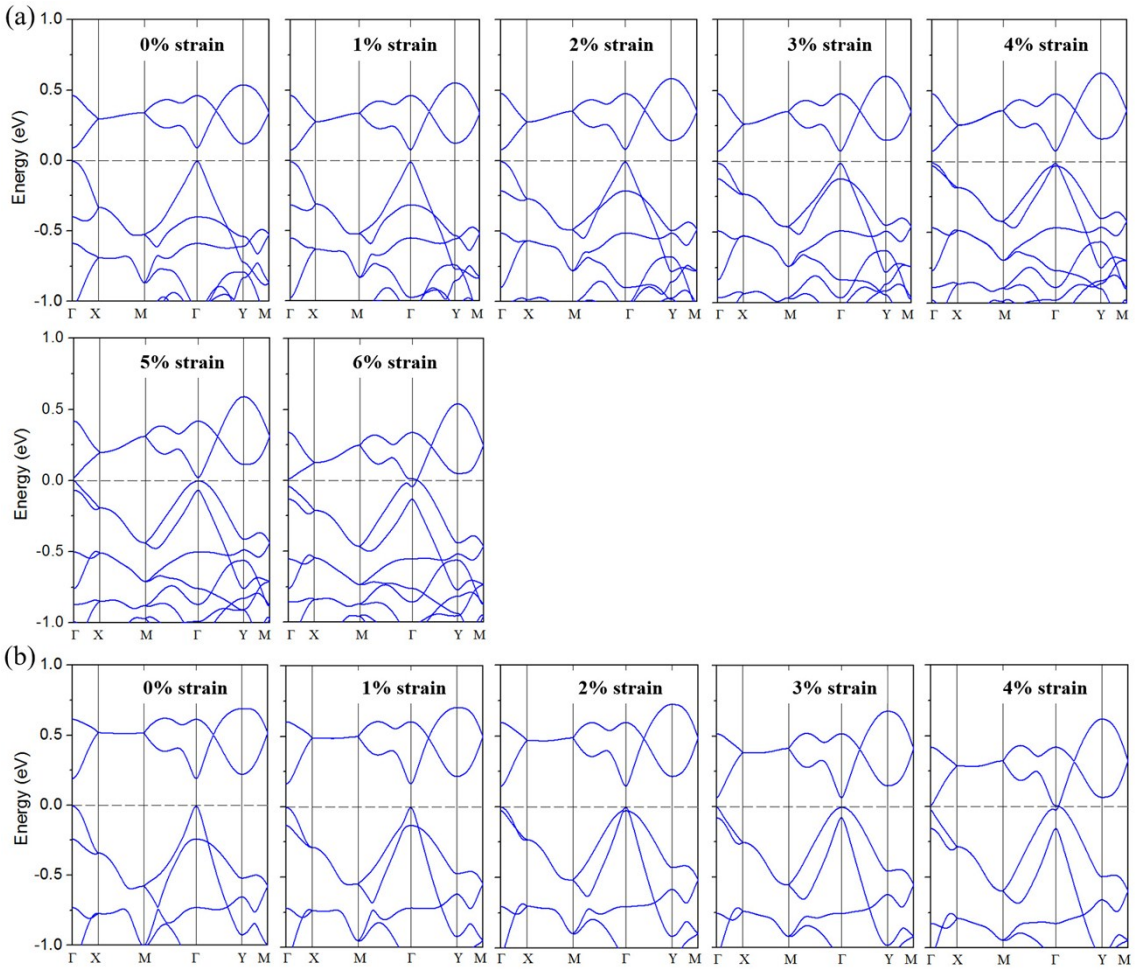

Figure S7. Electronic band structure of (a) sho-$MoSe_2$ and (b) sho-WS_2 under different magnitudes of equi-biaxial tensile strain (at the PBE level).

Table S1. Optimized lattice parameters and electronic band gaps E_g at the PBE level for sho-MX_2 structures, where M = Mo and W, and X = S, Se and Te.

sho-MX_2	a (Å)	b (Å)	E_g (eV)
MoS_2	9.98	5.70	0.35
$MoSe_2$	10.41	5.92	0.10
$MoTe_2$	11.12	6.18	metallic
WS_2	10.02	5.73	0.20
WSe_2	10.42	5.92	metallic
WTe_2	11.08	6.18	metallic

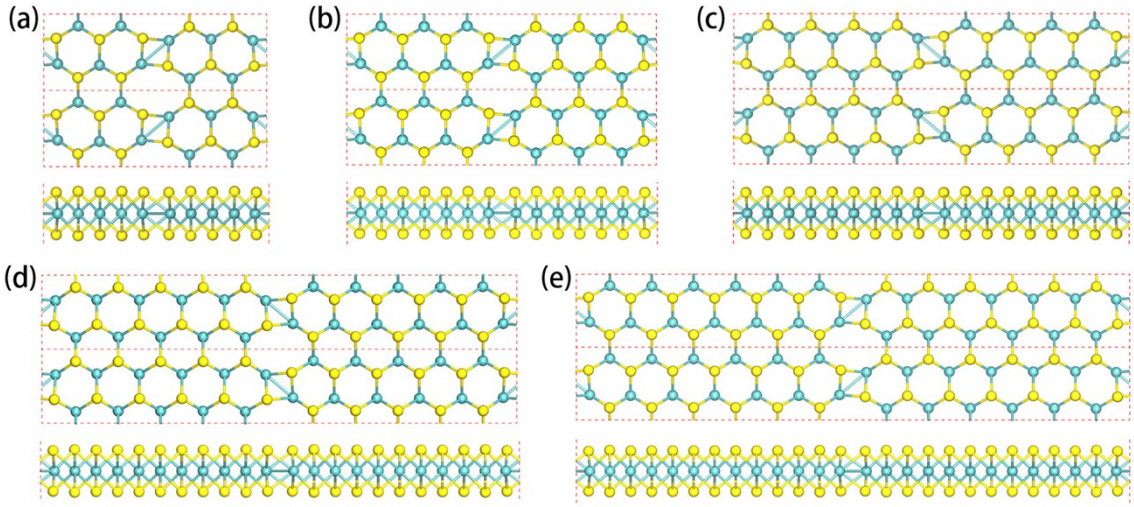

Figure S8. Optimized structures of (a) sh^{2}o-MoS_2, (b) sh^{3}o-MoS_2, (c) sh^{4}o-MoS_2, (d) sh^{5}o-MoS_2, and (e) sh^{6}o-MoS_2 from the top and side views.

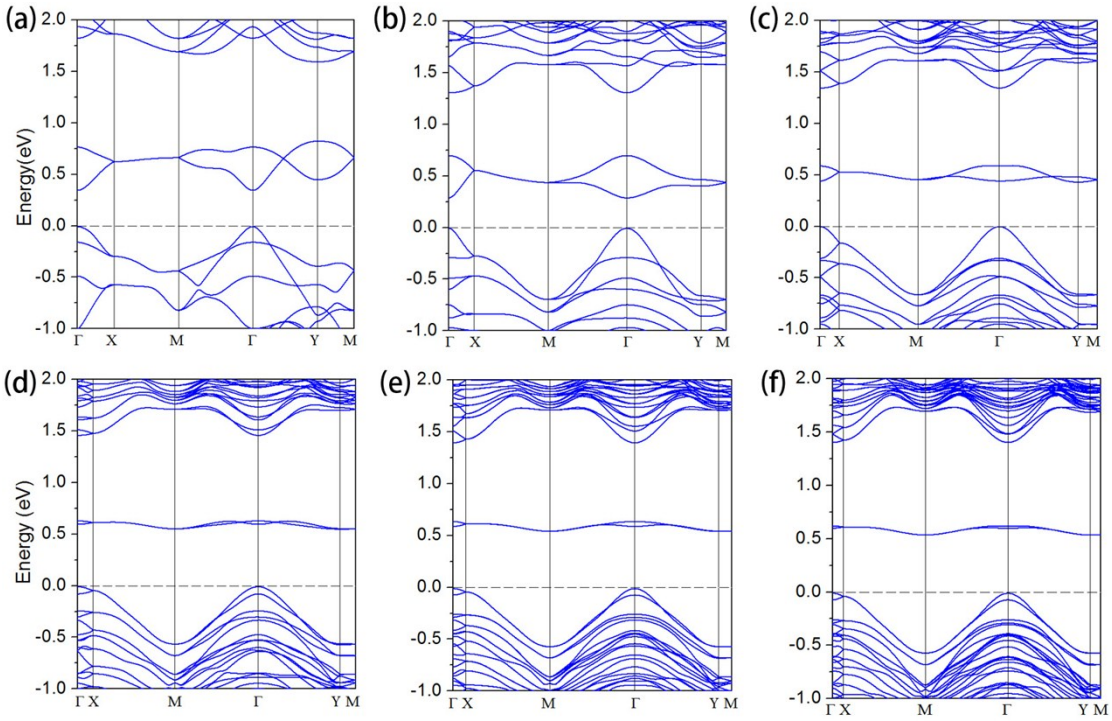

Figure S9. Electronic band structure of (a) sho-MoS_2, (b) sh^2o-MoS_2, (c) sh^3o-MoS_2, (d) sh^4o-MoS_2, (e) sh^5o-MoS_2, and (f) sh^6o-MoS_2 at the PBE level.

From the results in Table S2, one can see that the band gaps of sh^no-MoS_2 structures increase as the value of n increases except for the case of n = 1. This can be attributed to the structure uniqueness of sho-MoS_2. It is found that the charge is mainly distributed in the octagon rings by calculating band-decomposed charge density corresponding to the two lowest unoccupied bands of sh^no-MoS_2. For sh^no-MoS_2 with n value larger than 1, where the neighboring octagons are separated by hexagons along the crystal axis a, so that suppressing the interaction of localized charge in two neighboring octagons. However, for sho-structure, there is no hexagon unit between the neighboring octagonal rings along the crystal axis a, thus the charge localized in the neighboring octagons can directly interact with each other, resulting in the abnormal value of band gap.

Table S2. Optimized lattice parameters, relative energy (E) calculated with respect to H-MoS_2, and band gap (E_g, calculated by using the PBE functional) for sh^{n}o-MoS_2 (n=1-6).

n in sh^{n}o-MoS_2	a (Å)	b (Å)	E (eV/f.u.)	E_g (eV)
1	9.98	5.70	0.60	0.35
2	16.40	5.60	0.37	0.29
3	22.80	5.56	0.27	0.43
4	29.18	5.55	0.21	0.56
5	35.54	5.54	0.17	0.55
6	41.91	5.54	0.15	0.55

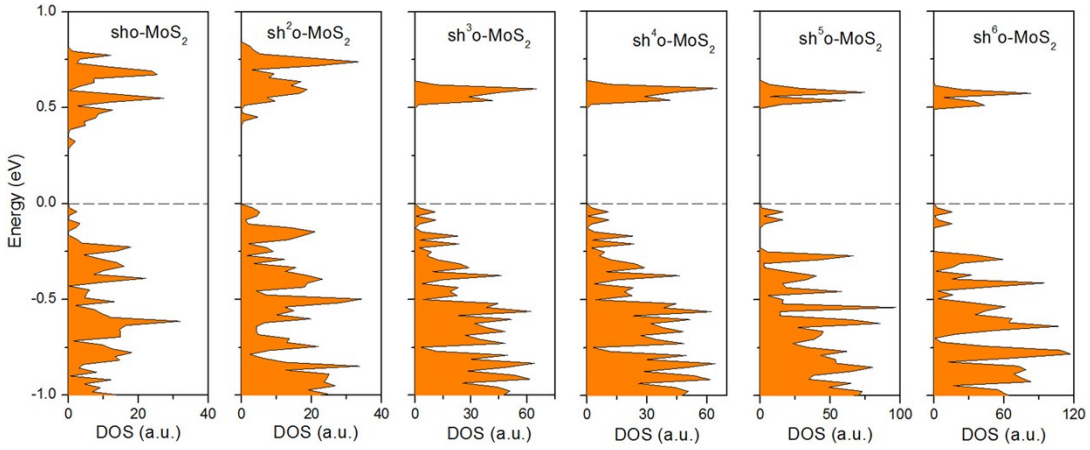

Figure S10. Electronic density of states (DOS) of sho-, sh^{2}o-, sh^{3}o-, sh^{4}o-, sh^{5}o-, and sh^{6}o-MoS_2. Here a.u. represents arbitrary unit.

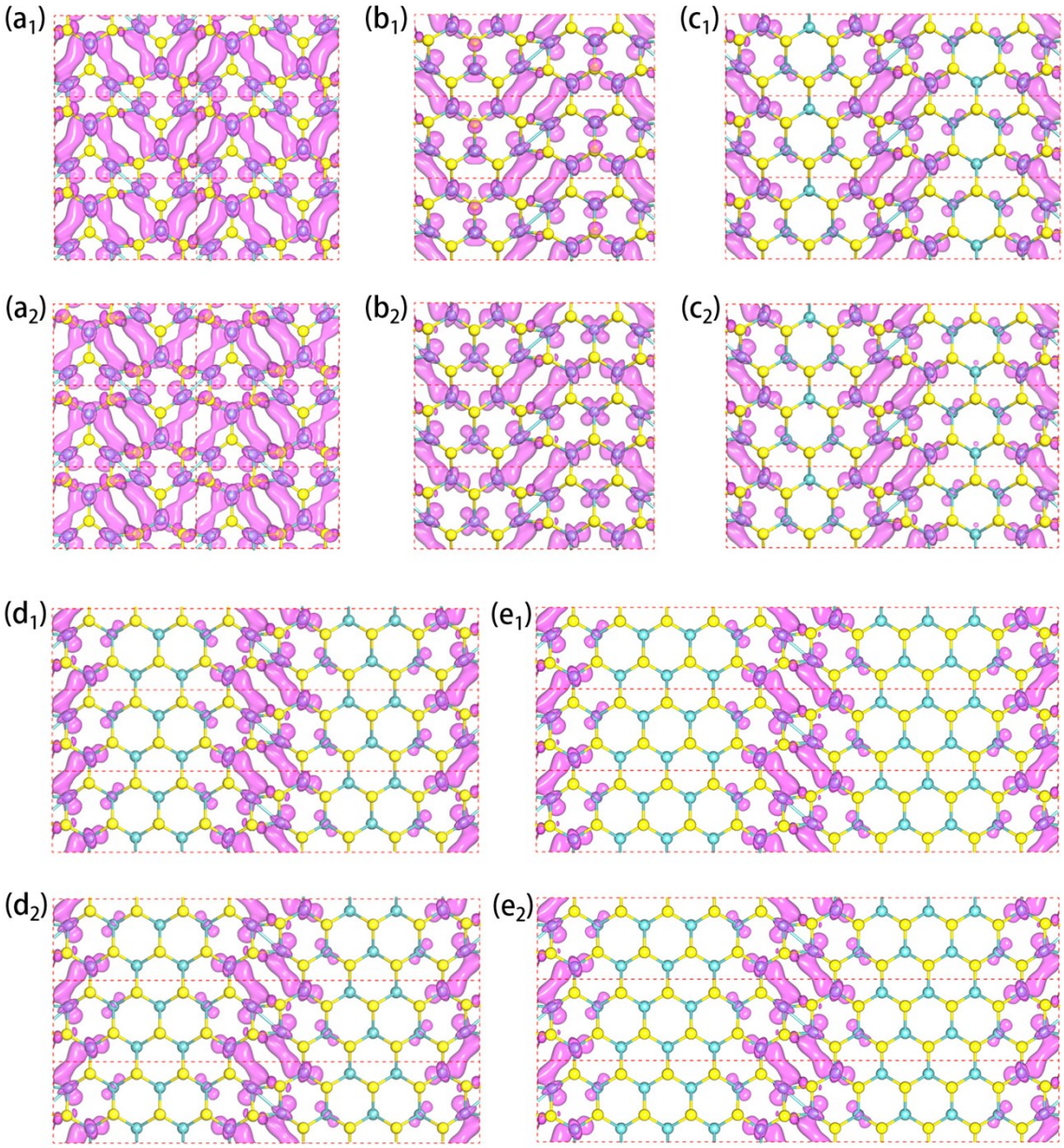

Figure S11. Band-decomposed charge density isosurfaces (isovalue: 0.01 e/Å^3) corresponding to the lowest and the second lowest unoccupied energy bands of sh^{n}o-MoS_2: (a_1) and (a_2) for sho-MoS_2; (b_1) and (b_2) for sh^{2}o-MoS_2; (c_1) and (c_2) for sh^{3}o-MoS_2; (d_1) and (d_2) for sh^{4}o-MoS_2; (e_1) and (e_2) for sh^{5}o-MoS_2. The top and bottom panels are the charge of the lowest and second lowest unoccupied bands, respectively.